



*Conference Proceedings Paper – Remote Sensing*

## Multi-Temporal Pixel Trajectories of SAR Backscatter and Coherence in Tropical Forests

Elsa Carla De Grandi <sup>1,\*</sup>, Edward Mitchard <sup>1</sup>, Astrid Verhegghen <sup>2</sup>,  
Dirk Hoekman <sup>3</sup> and Francesco Holecz <sup>4</sup>

<sup>1</sup> University of Edinburgh, School of GeoSciences, Crew Building, The King's Buildings, Alexander Crum Brown Road, Edinburgh EH9 3FF; E-Mails: E.De-Grandi@sms.ed.ac.uk (E.C.D.G); edward.mitchard@ed.ac.uk (E.M).

<sup>2</sup> European Commission, Joint Research Centre, Institute for Environment and Sustainability, Via E. Fermi 2749, 21027 Ispra (VA), Italy; E-Mail: astrid.verhegghen@jrc.ec.europa.eu (A.V.).

<sup>3</sup> Wageningen University, Droevendaalsesteeg 3, 6708 PB, Wageningen, The Netherlands; E-Mail: dirk.hoekman@wur.nl (D.H.)

<sup>4</sup> sarmap SA, Cascine di Barico 10, 6989 Purasca, Switzerland. E-Mail: fholecz@sarmap.ch.

\* Author to whom correspondence should be addressed; E-Mail: E.De Grandi@sms.ed.ac.uk; Tel.: +44 (0) 131 650 5103 (ext. 123); Fax: +44 (0) 131 662 0478.

*Published: 6 June 2015*

---

### Abstract:

Tropical forest natural and anthropogenic changes can be tracked using a pixel based time-series analysis of multi-temporal Interferometric Synthetic Aperture Radar (InSAR) backscatter and coherence provided by TanDEM-X. A pixel trajectory is defined as a set of values of all resolution elements (backscatter or coherence) at the same row and column position in the stack of images. Analysis of the trajectories over an area by means of a set of parameters (features) that characterize its time evolution can give insight on the nature and changes of tropical forest due to disturbance events (e.g. deforestation and forest degradation) but also due to natural changes in environmental conditions (e.g. increased rainfall). The following set of trajectory features was computed: linear fitting (trend), dispersion around trend (RMSE), maximum change (swing), statistics of the trajectory finite difference at one step (variance and intermittency). Results indicate that linear regression parameters captured changes due to forest/non forest conversion with negative slope indicating clearing events. The study reports results from a highly disturbed tropical forest environment in the Republic of Congo.

**Keywords:** SAR; multi-temporal; pixel trajectories; tropical forest; deforestation.

---

## 1. Introduction

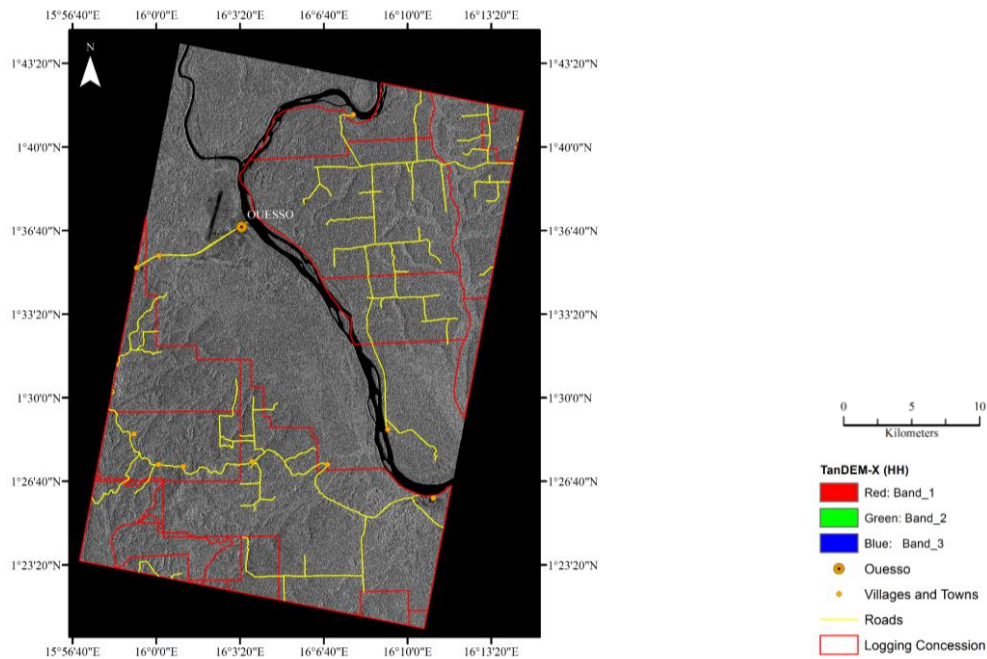
The Congo Basin hosts the second largest dense humid tropical forest in the world after the Amazon rainforest playing a crucial role in the global climate system and providing benefits in terms of livelihoods [1]. The role of tropical forests in international agreements such as the United Nations Framework Convention on Climate Change (UNFCCC) is critical and in particular for international initiatives such as Reducing Emission from Deforestation and Forest Degradation (REDD+). Forest disturbance mapping (deforestation and forest degradation) and monitoring in tropical forests of the Congo Basin is most efficiently accomplished using remote sensing. Mapping forest disturbance with the use of orbital Synthetic Aperture Radar (SAR) has many advantages over optical sensor due to the ability to penetrate cloud cover and haze and being independent of daylight conditions. The potential of the TanDEM-X mission has led to the unprecedented possibility to map tropical forests at high spatial resolution by providing interferometric coherence as well as backscatter. The importance of this data for tropical forest mapping and monitoring is highlighted in the present study with analysis of a multi-temporal stack of TanDEM-X scenes in a highly disturbed forest setting.

Net deforestation in Northern Congo (Likouala and Sangha provinces) has been estimated to 0.03% for the period between 2000-2010 mainly due to increased use of forest resources and population growth [1]. The greatest forest loss in the study area occurred between 1990 and 2001 around Ouesso giving rise to a mosaic of secondary forest and agriculture [1]. Other factor that contribute to the removal of vegetation include selective logging for commercial purposes.

## 2. Study Site

The analysis focuses around the city of Ouesso, Republic of Congo (UL: 15° 56'20.02'' E, 1° 44'42.83'' N) and covers 25 x 40 km (Figure 1). The area is dominated by dense humid evergreen forest from the Guinean Congolese region (with areas affected by selective logging and thus variations from closed to more open canopy cover due to level of disturbance undergone in the past) and swamp forest around the Sangha river. The site is prone to a high level of disturbance for instance in proximity of urban centers where, clearing for agricultural purposes and shifting cultivation is extensive. The clearings are on average no larger than 1 ha and are concentrated around the city of Ouesso and Mboko and along the N2 road network. The Ngombe and Pokola logging concession are also situated within the study site where, exploitation of forest through selective logging has been undertaken on rotation between 1985 and 2008 but has now stopped. The impact is still detectable visually by the presence of old logging roads in certain areas. However, rapid forest recovery is proving difficult to identify areas where logging occurred in the past.

**Figure 1.** Study sites location near Ouesso, Republic of Congo (RoC).  
Data Source: World Resources Institute and DLR.



### 3. Dataset and Processing

Six TanDEM-X StripMap scenes (supplied by DLR through the VEGE03030 AO) were acquired between 2012 and 2014, at HH polarization,  $47^\circ$  incidence angle and descending mode. The data was processed using SARscape software (5.0) [2] and included the following steps: a) multi-looking (2 range and 2 azimuth looks, corresponding to a slant range pixel size of  $3.69 \times 3.73$  m); b) interferometric workflow (interferogram generation and flattening, adaptive local frequency filter and coherence generation); c) co-registration d) multi-temporal filtering e) geocoding in a Geo-Global Lat/Lon system with  $3.33 \cdot 10^{-5}$  degree pixel size (approximately 4 m). Both the backscatter (power) and the coherence datasets were co-registered and filtered to reduce noise (speckle and coherence estimator variance) using the multi-temporal filter implemented in SARscape and based on the principle proposed in [3].

We recall the definition of interferometric coherence:

$$\gamma = \frac{\langle S_1 S_2^* \rangle}{\sqrt{\langle |S_1|^2 \rangle \langle |S_2|^2 \rangle}} \quad (1)$$

Where:

$|\gamma|$  = Complex coherence

$\langle \dots \rangle$  = Ensemble Average

$S_1, S_2$  are the complex slant range images acquired by the two Tandem instruments. The absolute value of coherence  $|\gamma|$  is used in the following.

Very High Resolution data acquired in December 2013 available from Google Earth, and accumulated precipitation data from Tropical Rainfall Measuring Mission (TRMM) were used as ancillary reference data. Visual interpretation based on ancillary knowledge was used for training of the supervised analysis. Selected thematic classes are: closed evergreen tropical forest, swamp forest, agriculture and grassland. It is important to note, in the context of the time-series analysis performed in this work, that the class definition corresponds to the situation at some days before  $t4$  (December, 17th, 2013), which is the date of the available Google Earth dataset with the highest spatial resolution. The TanDEM-X datasets acquisition dates and the TRMM rainfall data at 48 h before the SAR acquisition time are summarized in Table 1. Notice that that the highest precipitation occurred at  $t5$ .

**Table 1.** Multi-temporal stack used to compute multi-temporal pixel trajectories.

<b>Time</b>	<b>Date</b>	<b>Rainfall (mm)*</b>
$t1$	05-Dec-2012	0
$t2$	14-Mar-2013	0.587
$t3$	15-May-2013	20.657
$t4$	25-Dec-2013	7.603
$t5$	03-Apr-2014	29.843
$t6$	06-May-2014	12.382

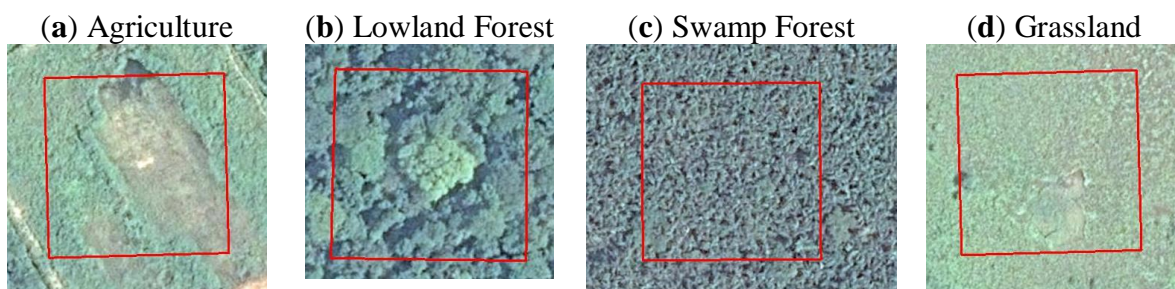
\*based on TRMM data for a period of a 48 h before the date of acquisition.

## 2. Methods

### 2.1 Supervised Analysis

Analysis was undertaken, in the first instance, on four 15x15 pixels areas on interest (AOI). The areas were selected based on ancillary information (LANDSAT and high resolution Google Earth imagery and previous knowledge of the area). Figure 2 shows the four AOI on a high resolution Google Earth scene (December, 17<sup>th</sup> 2013).

**Figure 2.** Areas of Interest (AOI) used for the analysis on Very High Resolution Google Earth imagery acquired on December 17<sup>th</sup>, 2013 (Google Earth, 2013).



## 2.2 Multi-temporal Pixel Trajectories

A pixel trajectory is defined as a set of values of all resolution elements at the same row and column position in the stack of images. The following set of trajectory features were computed on either the multi-temporal backscatter stack or multi-temporal coherence: a) Trend analysis by linear regression (line intercept, slope and coefficient of determination and deviations from the trend); b) Swing c) Variance of the de-trended trajectory's finite differences at 1 step and d) Maximum of the absolute value of the finite difference vector.

a) Trend analysis by linear regression of  $P_j(j = 1..n)$ , where P is the pixel value at date j, n is the number of dates in the multi-temporal stack. This step yields the fitting line with two parameters (slope m and intercept c), and the root mean squared deviations of the points from the line:

$$y(k) = c + m k \quad (2)$$

$$\nabla Prms = \sqrt{\sum_{k=1}^n (P(k) - y(k))^2} \quad (3)$$

b) Swing:

$$\max(P_j) - \min(P_j) \quad (4)$$

c) Variance of the de-trended trajectory's finite differences at 1 step (a measure of departure velocity from trend) :

$$Pdt(k) = P(k) - y(k) \quad (5)$$

$$d(k) = Pdt_{k+1} - Pdt_k \quad (6)$$

$$VD = \log \left( \frac{1}{n-1} \sum_{k=1}^{n-1} d^2(k) - \left( \frac{1}{n-1} \sum_{k=1}^{n-1} d(k) \right)^2 \right) \quad (7)$$

d) Maximum of the absolute value of the finite difference vector (a measure of large intermittent events):

$$Md = \text{Max}(d(k)) \quad (8)$$

## 3. Results and Discussion

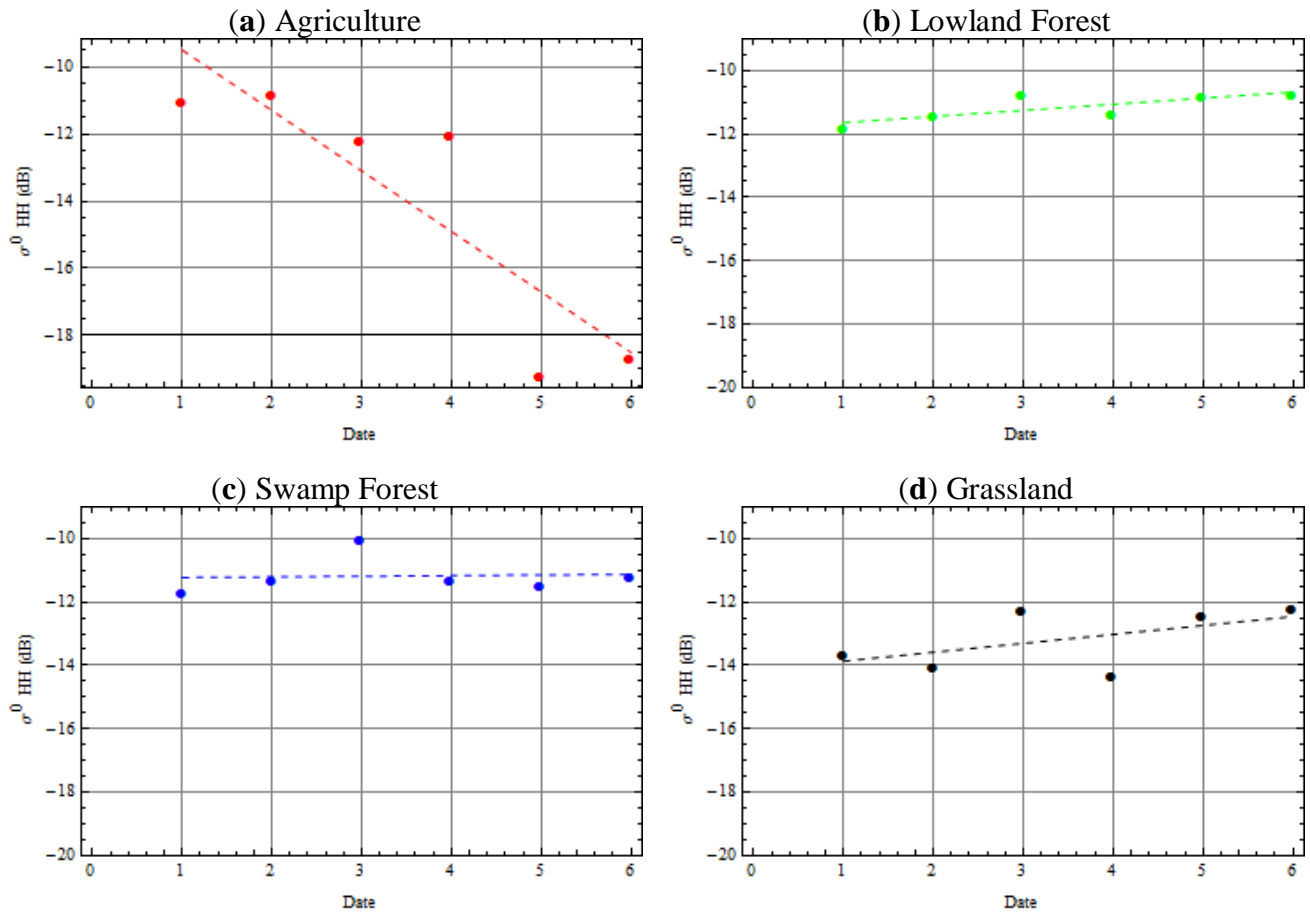
### 3.1. Multi-temporal Pixel Trajectories of SAR backscatter

Results indicate that multi-temporal pixel trajectories pick up changes related to: (i) environmental conditions (effect seasonality and rainfall) and (ii) disturbance events such forest disturbance (deforestation).

Radar cross section (RCS) (Figure 3) for the 4 AOI indicates that the variations for lowland forest and swamp forest are not as marked as those for agriculture and grassland. The changes in lowland forest (values ranging from -10.7 dB to -11.8 dB over time) and swamp forest (values ranging from -10.0 dB to -11.7 dB over time) can be mainly attributed to changes in environmental effects (e.g. moisture) and not due to anthropogenic disturbance such as clearing. While, a greater change in RCS is noticeable for the agriculture and grassland, this being a consequence of anthropogenic disturbance (especially for the class agriculture with RCS ranging between -10.8 dB and -19.2 dB). The RCS for grassland goes from of -14.3 dB to -12.2 dB.

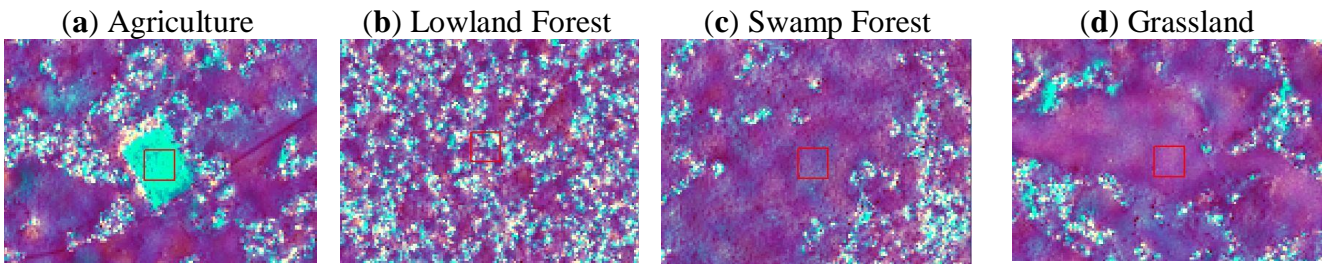
Lowland forest presents high RCS throughout the time series with no significant sign of disturbance since the area is situated far from the main villages and towns, outside of the logging concessions. However, there is a noticeable fluctuation in RCS for this class due to rainfall events, these changes being all  $< 1$ dB. Swamp forest also presents small fluctuations in RCS ( $< 1$ dB), these being also attributable to the impact of environmental conditions. Grassland also undergoes changes especially at date 3 where RCS is highest -12.2 dB with subsequent decrease to -14.3 dB. The changes which are occurring within this AOI are  $> 1$ dB for dates 2&3, 3&4 and 4&5. The high RCS is attributable to the presence of taller grass which is then cleared and converted into bare field in preparation for agriculture conversion with the underlying influence of moisture conditions also contributing to the RCS (Figure 3d).

Analysis of multi-temporal pixel features within an AOI (Figure 4) provide extra information to understand the RCS dynamics for the 6 dates (Table 3). The swing (difference between maximum and minimum in the stack) is highest for the class agriculture, because of the abrupt change due to conversion from vegetation to agriculture at date  $t_5$ , as suggested by Figure 3a. Instead, the swing for both the lowland forest and the swamp forest is the lowest. This feature indicates that the most dynamic classes are agriculture and grassland. The slope of the linear fit line also suggests that the trend in the class agriculture is very strong and negative (-60.9) while, the slope for the other 3 classes is positive with swamp forest having the lowest slope (1.1). The RMSE is highest for the class agriculture (1.7) and lowest for the lowland forest class (0.25). The variance of the finite differences is much higher for the class agriculture compared to all the other AOI. The same applies for the maximum absolute value of the differences, with 10.5 and 29.0 respectively.

**Figure 3.** Radar Cross Section (RCS) linear regression for four AOI.**Table 2.** Multi-temporal features statistics (mean) for four AOI (a) agriculture; (b) lowland forest; (c) swamp forest and (d) grassland.

Feature	(a)	(b)	(c)	(d)
Swing	8.3	1.1	1.6	2.0
Trend Slope	-60.9	10.9	1.1	15.7
Deviations from trend (RMSE)	1.7	0.2	0.5	0.7
Variance	10.5	0.2	0.9	2.6
Intermittency	29.0	0.5	1.7	5.2

**Figure 4.** Multi-temporal features colour composite (R= slope, G= swing and B= Variance).for four 15 x 15 pixel AOI. (a) agriculture; (b) lowland forest; (c) swamp forest and (d) grassland.



### 3.2 Multi-temporal Pixel trajectories of Coherence

Analysis of coherence for the same AOI revealed interesting patterns (Figure 5 and 6). Coherence for class agriculture reveals that this is high until  $t_5$  (0.72) (April 2014), this being the date which is affected by highest precipitation. On the next date  $t_6$  coherence remains low (0.7). The reason for the drop in coherence could be due to the effect of vegetation regrowth in an area which was previously cleared for agricultural practice, and/or the possibility of the area to be flooded. Regarding the first hypothesis, notice that a sparse vegetation layer would afford enough penetration at X-band as to increase dramatically volume decorrelation. In contrast, for a dense homogeneous forest, such as the swamp, only a thin layer of the top canopy would be interested in volume decorrelation, thus yielding high values of coherence. The low values of coherence in this area are also matched by low RCS value. This situation calls for scattering elements properties in the vegetation layer where absorption dominates over scattering.

Lowland forest presents coherence which is lower than all the other classes apart at  $t_2$  where it is slightly above coherence for class grassland and the two cases where the class agriculture presents very low coherence at  $t_5$  and  $t_6$ . Lower coherence for lowland forest is to be expected, because of the spatial modulation of the amount of scatters in the volume (emergent trees, several competing species), which causes decorrelation of the signal. Instead, swamp forest has a much more homogeneous canopy cover with smaller tree crowns and therefore, coherence is almost always higher compared to other classes. An exception is date  $t_5$ , where class grassland presents the highest coherence values. At this point in time, the area of class grassland could have been cleared for agriculture purposes and thus gives rise to lower coherence values (0.92).

**Figure 5.** TanDEM-X coherence (R= 12/2012, G= 12/2013 and B= 05/2014) for four 15 x 15 pixel AOI. (a) agriculture; (b) lowland forest; (c) swamp forest and (d) grassland.

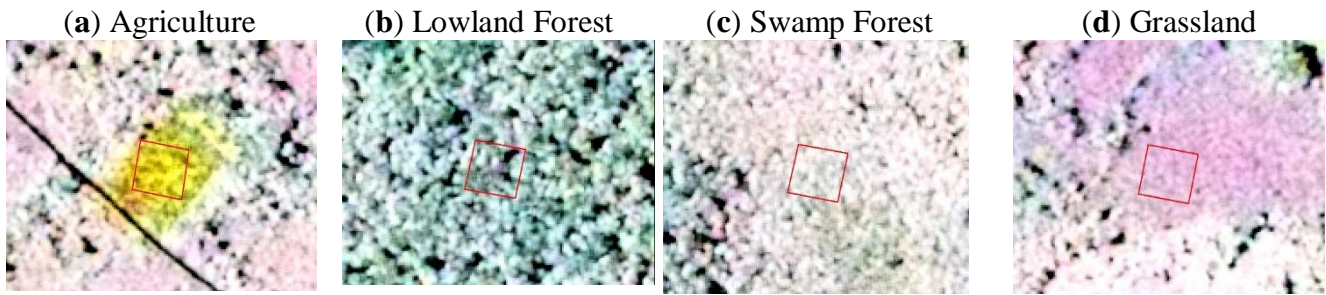
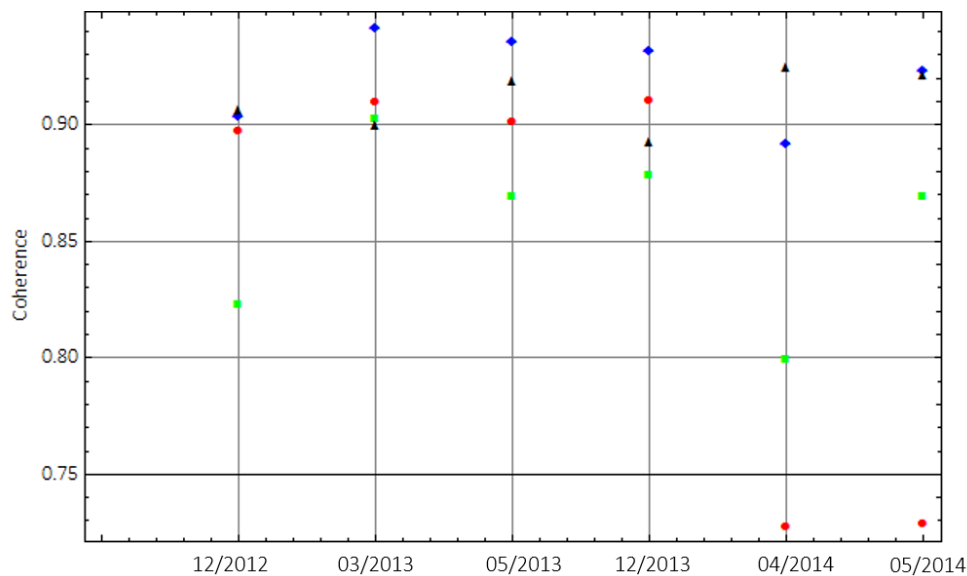


**Figure 6.** TanDEM-X coherence trajectory from December 5th, 2012 to May 6th, 2014 for (a) agriculture (red); (b) lowland forest (green); (c) swamp forest (blue) and (d) grassland (black).



#### 4. Conclusions

Results indicated that the use of multi-temporal pixel trajectories in InSAR imagery is a useful tool to follow the evolution of natural targets. However, it is important to distinguish between natural changes due to seasonality and environmental conditions (e.g. rainfall), as in the case of results provided for lowland tropical forest and swamp forest, and changes due to anthropogenic disturbance (conversion from forest to non-forest). It was found that the features are able to characterize for instance the conversion from forest to non-forest (deforestation) for agriculture purposes. The slope of the linear trend indicates the magnitude of the change and whether the trend is positive (vegetation regrowth) or negative trend (deforestation). The analysis will be extended in particular to look at areas which present a negative trend as a means to provide estimates of deforestation.

## Acknowledgments

The authors would like to thank DLR for the provision of TanDEM-X data through AO proposal VEGE03030. The authors would like to acknowledge the funding bodies: the University of Edinburgh and the School of GeoSciences.

## Author Contributions

The data analysis was undertaken by E.C.D.G and E.M.. A.V. contributed with her knowledge on tropical forest in the Republic of Congo. F.H. provided software and help with data processing.

## Conflicts of Interest

The authors declare no conflict of interest.

## References and Notes

1. de Wasseige, C.; Flynn, J. ; Loupp, D.; Hiol, F. and Mayaux, P. Title of the chapter. In *The Forests of the Congo Basin- State of the Forests 2013.*, Publisher: Belgium, Country, 2014; pp. 328.
2. The SAR Guidebook. [http://www.exelisvis.com/portals/0/pdfs/envi/SAR\\_Guidebook.pdf](http://www.exelisvis.com/portals/0/pdfs/envi/SAR_Guidebook.pdf) (accessed on May 20th 2015).
3. De Grandi, G.F.; Leysen, M.; Lee, J.S. and Schuler, D. *Radar reflectivity estimation using multiple SAR scenes of the same target: Technique and applications.* In Proc. IEEE Int. Remote Sens. Sci. Vis. Sustain. Develop. Geosci. Remote Sens. (IGARSS'97), Aug. 3–8, 1997, vol. 2, pp. 1047– 1050.

© 2015 by the authors; licensee MDPI, Basel, Switzerland. This article is an open access article distributed under the terms and conditions of the Creative Commons Attribution license (<http://creativecommons.org/licenses/by/4.0/>).